



Hydrogen production via hydrolysis of Al–eutectic GaInSn composites

Gang-qiang LIANG^{1,2}, Yuan LIU^{1,2}, Peng-fei CHEN^{1,2}, Can-xu ZHOU^{1,2}, Tan WAN^{1,2}

1. School of Materials Science and Engineering, Tsinghua University, Beijing 100084, China;

2. Key Laboratory for Advanced Materials Processing Technology, Ministry of Education, Beijing 100084, China

Received 15 March 2022; accepted 4 July 2022

Abstract: A novel way of constant hydrogen generation via Al and liquid metal eutectic GaInSn (eGIS) was proposed. The cylindrical Al with a blind hole served as a container of liquid metal to generate hydrogen via hydrolysis, while eGIS was considered a window for triggering the reaction. The microstructure, hydrolysis evolution and hydrogen production performance of the semi-solid Al–eGIS composites were investigated. The results indicated that the liquid metal embrittlement occurs when the eGIS diffuses along the grain boundaries of polycrystalline Al, which increases the reaction activity of the composites; while the formation of In₃Sn and InSn₄ secondary phases was observed, which accelerated the hydrolysis of Al. Moreover, the Al–10wt.%eGIS and Al–20wt.%eGIS composites achieved nearly 100% conversion yield of hydrolysis. Consequently, the samples were practically applied to proton exchange membrane fuel for performance measurement, with a stable power supply of 0.54 W for 110 min.

Key words: hydrogen production; hydrolysis; Al-based composite; liquid metal

1 Introduction

As an energy-storage material, aluminium possesses outstanding volumetric and gravimetric energy density, at 31.1 MJ/kg and 83.8 MJ/L, respectively. Such a stored chemical energy is expected to be used to generate H₂ via hydrolysis. As a light metal, 1 g of Al at 25 °C and atmospheric pressure reacts with water to theoretically produce 1361.1 mL of H₂ (Reaction (1)), with a gravimetric density and volumetric density of 3.732 wt.% and 47.215 g/L including water, and 11.206 wt.% and 302.562 g/L excluding water, respectively. The production of high purity H₂, and the release of vapor and heat suggest that integrated water and thermal management between the Al–water reaction unit and the fuel cell is valuable. This meets the U.S. Department of Energy (DOE) targets for gravimetric capacity systems at 7.5% (kg H₂/kg) and volumetric capacity systems at 70 g/L relative

to H₂ with a fuel purity of 99.97% [1]. However, the Al–water reaction does not proceed owing to the adherent and compact aluminium oxide film that forms on the surface of aluminium particles, which impedes subsequent reaction because fresh Al fails to be exposed to water.



Continuous hydrolysis is basically achieved by two main effective approaches: the mechanical activation (ball-milling and mechanochemical treatment) with low melting point metals/alloys [2–4], alloying elements [5,6], non-metal elements [7], salts [8,9], metal hydrides [10], alkali [11] and metallic oxides [12]; high-temperature processing (arc-melting, casting and melt-spinning, and gas-atomization processing) with low melting point metals/alloys [13–17], alloying elements [18,19], or a combination of these methods to form a complex Al composite [20–22]. However, these two traditional methods basically

involve high energy consumption, time-consuming issues, flammable, and explosive powders and a caustic environment.

Liquid Ga-series alloys have been proven to be effective activators of the Al–water reaction by preventing the coherent formation of the thin passivation film through the creation of surface active sites. In previous research, the activation of Al–water reaction by Ga-series alloys basically involves high-temperature melting or high energy ball-milling. For Al–Ga, Al–In, Al–Sn, and Al–Ga–Sn alloys, no H₂ is produced from tap water at room temperature when the alloy element mass fraction is less than 10%. However, Al–Ga–In and Al–In–Sn alloys can directly react with tap water at room temperature. Compared with ternary activated Al systems, the activity of quaternary Al–Ga–In–Sn alloy is greatly improved [2]. All Al–In–Sn ternary alloys exhibit poor hydrolysis activity at room temperature. Al–In–Sn alloy will represent the highest hydrogen yield when the mass ratio of In to Sn is 1:4. The hydrolysis activity of Al alloys is greatly improved while Ga is introduced to the ternary alloys [14]. HUANG and SHU [13] quenched AlGaInSn alloy with semi-solid structures by melting Al with 15 wt.% 62Ga25In13Sn, remelting at 620 °C for 120 min to obtain a semi-solid slurry, and then quenching in liquid nitrogen to obtain a semi-solid metal, obtaining 50 mL H₂ in 10 min. However, conventional activation methods still face deficiencies such as high energy consumption and complex processes. Hence, avoiding ball milling and melting is necessary for the hydrolysis activation of Al–Ga alloys.

Recently, YU et al [23] reported semi-solid Al–Ga composites that underwent direct hydrolysis with H₂ generation, which was fabricated by mixing liquid Ga and fragmented Al foils at room temperature under stirring with a glass rod for only a few minutes instead of melting at hundreds of degrees for a long period. XU et al [24] prepared 0.2 g of Al activated by 4 g of Ga–In–Sn–Bi alloy for hydrolysis in 0.4 mol/L NaCl solution, which yielded at 92% hydrogen productivity. However, the mass ratio of Al stays relatively low, which means less hydrogen production yield. Hence, we aimed to propose a convenient method for hydrogen production from Al–water reaction using cuplike Al and eutectic GaInSn (eGIS) with the

mass fractions of Al exceeding 80%. The microstructure of the Al–eGIS composites, the typical hydrolysis process and the hydrogen production performance were investigated. Eventually, the Al–eGIS composites were applied to a proton exchange membrane fuel cell (PEMFC) for the evaluation of practical scenarios.

2 Experimental

2.1 Sample preparation

Bulk aluminium (composition in wt.%: 99.7 Al, 0.12 Fe, 0.08 Si, 0.04 Ca, 0.03 Mg and 0.03 Zn) was designed as a cylindrical cup (radius 7.5 mm and height 15 mm) with a central cylindrical blind hole (radius 2.5 mm and depth 10 mm), with an average mass of 6.5 g (Fig. 1). Before use, the passivated film of the blind hole was removed by etching for 15 s with 0.5 mol/L NaOH, where eGIS (99.99% purity; Ga/In/Sn mass ratio 62:22:16) in different mass fractions (5, 10 and 20 wt.%) was immediately transferred into it. The eGIS was recycled from hydrolysis by-products by centrifuging at 1400 r/min for 10 min and then the liquid metal at the bottom of the centrifugal tube was separated. After 0.5 mol/L NaOH washing to ensure the removal of residual Al and Al(OH)₃, the eGIS was transferred to the filter paper and weighed after air drying.

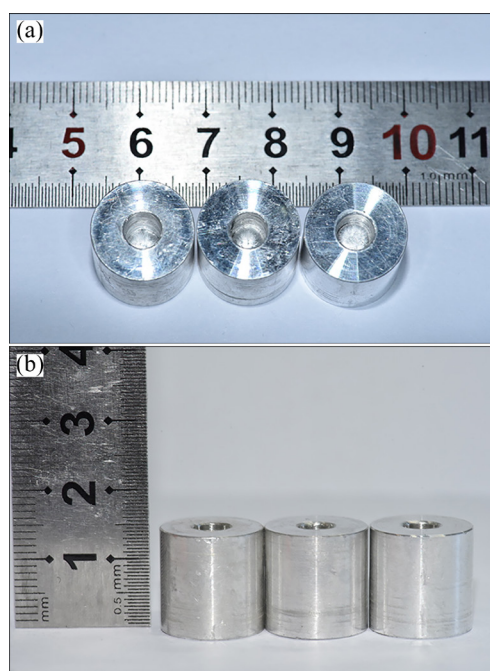


Fig. 1 Photos of samples (Al–5wt.%eGIS (left), Al–10wt.%eGIS (middle) and Al–20wt.%eGIS (right))

2.2 Characterization of samples

The microstructure of Al-based composites was detected by field emission scanning electron microscopy (FESEM; Gemini 500, Carl Zeiss AG, Germany) in backscattered electron (BSE) mode with elements analyzed by energy-dispersive X-ray (EDX) analysis. To minimize rapid oxidation and hydrolysis with water vapor during removal, the wetted sample was placed in a sample chamber immediately after removing the liquid metal. Differential scanning calorimetry (DSC; TA instruments Q5000IR, USA) was used to detect the melting point (T_m) and freezing point (T_s) of samples in the range from -50 to 150 °C. The samples (15–50 mg) were measured under an argon atmosphere with heating and cooling rates of 10 °C/min. A digital CMOS camera (D810, Nikon, Japan) was used to capture the sample morphology at different reaction stages. The structure of the Al–eGIS interface was detected by X-ray microscopy (Xradia 620 Versa, Carl Zeiss AG, Germany) using laboratory diffraction contrast tomography (LabDCT Pro) for picture reconstruction. For these samples, the wetting process was extended to 24 h, the eGIS was poured out, and then the epoxy resin was immediately applied to the sample surface to avoid oxidation and hydrolysis. An Al gasket was placed under the sample to prevent its exposure to air.

2.3 Hydrogen generation performance test

The hydrolysis performance was tested by the drainage method (Fig. 2). A 500 mL Pyrex glass reactor was placed in a thermostat water bath to maintain a constant temperature, with tap water

provided by a 500 mL pressure-equalizing dropping funnel. For each experiment, the sample added into the flask was about 6.5 g, and 500 mL distilled water was injected for the reaction. In this work, we considered the waste heat and water management simulation that utilized the water discharged from the cathode of the fuel cell as the reaction medium for the hydrolysis. Hence, the reaction temperatures were moderated to be 50 – 90 °C (the water temperature range of PEMFC) [25]. Humid and warm H_2 was cooled by a graham condenser with a constant supply of recirculating cooled water provided by a pump. After drying H_2 by passing through a drying tower containing allochroic silica gel, the H_2 yield was stoichiometrically calculated by the volume of water displacement at ambient temperature (273 K, and 1.013×10^5 Pa), and the hydrogen production rate can be calculated by the derivative of H_2 yield with respect to the reaction time. All gas pipes were rubber, and the junctions of glass containers were smeared with vacuum silicone grease to obtain rigorous airtightness. Each testing was repeated at least three times, and the results were averaged.

3 Results and discussion

3.1 Characterization results of semi-solid Al–eGIS composites

The semi-solid layer surface morphologies of coexisting solid and liquid phases are shown in Fig. 3(a). Owing to inevitable oxidation, an oxide film formed on the Al solid phase. However, EDX elemental mapping showed that the Ga-rich liquid phase was not susceptible to oxidation and acted as

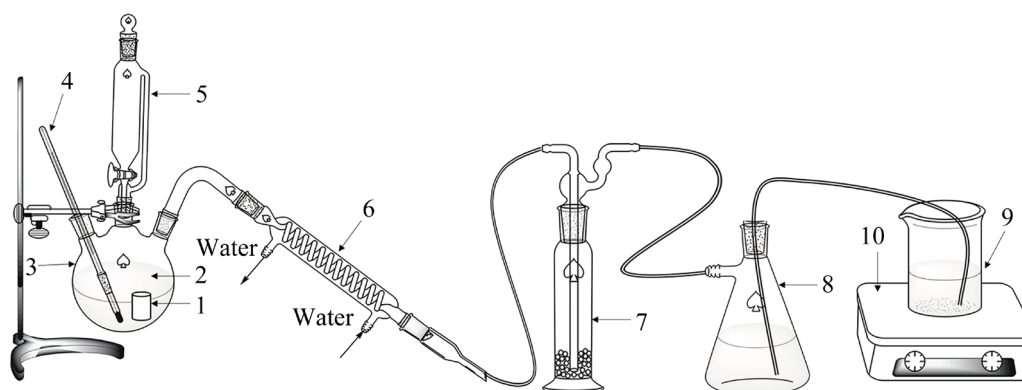


Fig. 2 Schematic diagram of drainage apparatus: 1—Sample; 2—Water; 3—Pyrex glass reactor with thermo-static water bath; 4—Thermometer; 5—Pressure-equalizing dropping funnel; 6—Graham condenser; 7—Drying tower containing allochroic silica gel; 8—Drainage flask; 9—Water container; 10—Electronic balance

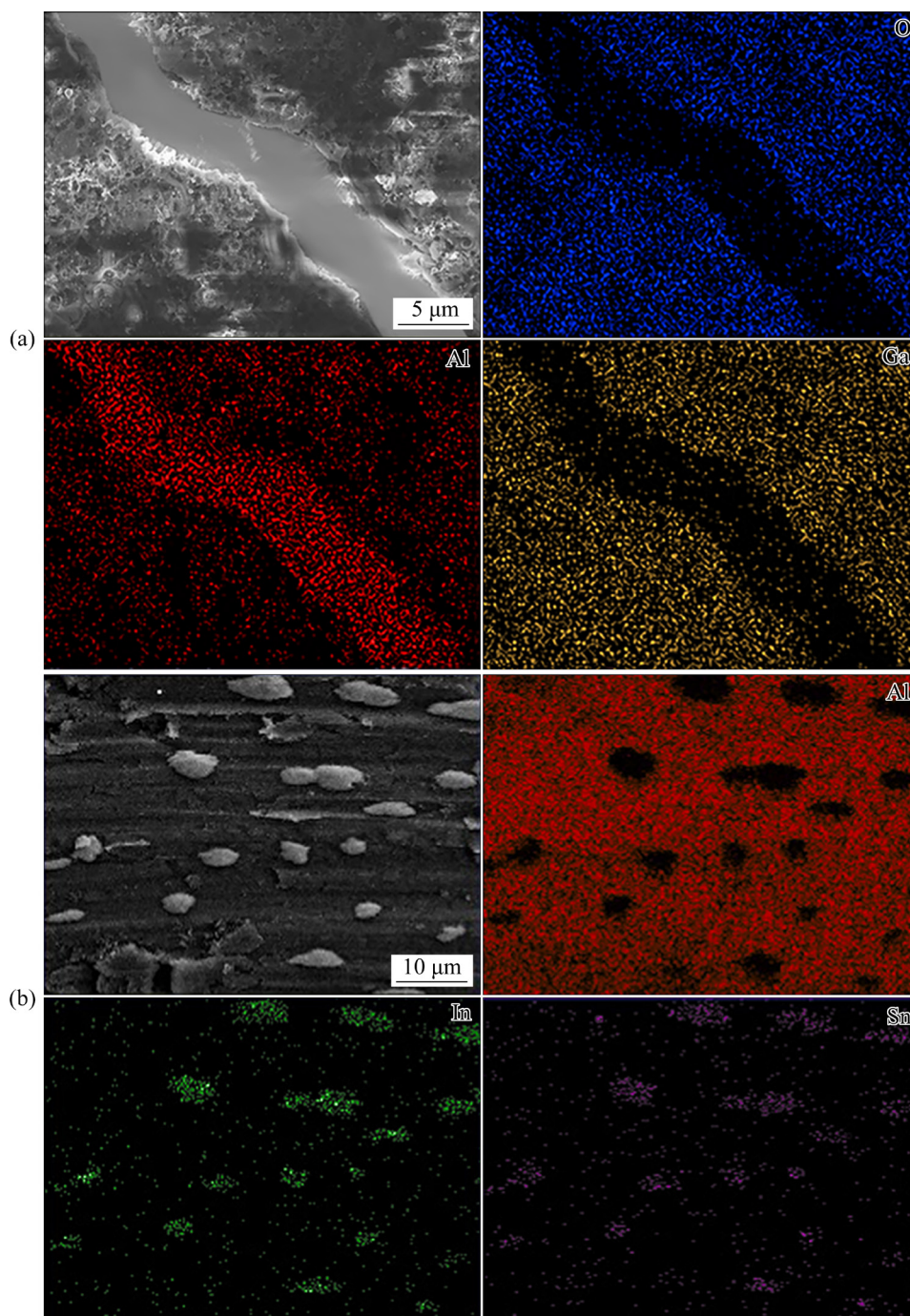


Fig. 3 BSE images and EDX mappings of surface morphology (a) and secondary phases (b) of semi-solid Al–eGIS composites

a window for hydrogen production. After scraping the shiny semi-solid layer from the surface, In–Sn second phase in the Al-rich solid phase was observed (Fig. 3(b)). It is well-known that the existence of liquid metal guarantees the wetting of Al.

Figure 4(a) shows the DSC curves of the Al–eGIS semi-solid composite during a heating and cooling cycle. The melting peak of the liquid phase

was observed at a T_m of 11.0 °C, which was slightly higher than the eutectic temperature of GIS (10.7 °C), due to the accuracy of DSC and the melting peak changed by Al in the eGIS liquid phase is small at the ambient temperature. Solidification started at 14.35 °C due to supercooling of the liquid phase. According to the X-ray diffraction results in Fig. 4(b), the 2θ values corresponding to the peaks of Al–Ga solid solution

are slightly declined compared to that of Al phase (PDF No. 04-0787), which indicates that Ga atoms diffuse into Al crystal lattice. The semi-solid Al-eGIS composite also contains intermetallic compound In_3Sn and InSn_4 phases.

The phenomenon of liquid metal embrittlement (LME) is caused by surface wetting and intergranular penetration of eGIS into polycrystalline Al with the loss of ductility without applied stress. The Al- x wt.%eGIS ($x=5, 10$ and 20)

composites follow the same typical hydrolysis. Here, the Al-10wt.%eGIS was represented in Fig. 5 to demonstrate the process. At the initial stage (Fig. 5(a)), a small number of hydrogen bubbles were generated from eGIS surface located in the blind hole, indicating the mass transfer of Al atoms into liquid metal. Some bubbles were clustered under the eGIS, causing the rising of liquid metal from the hole bottom to the top surface of cylindrical Al thanks to the buoyancy, and the shiny

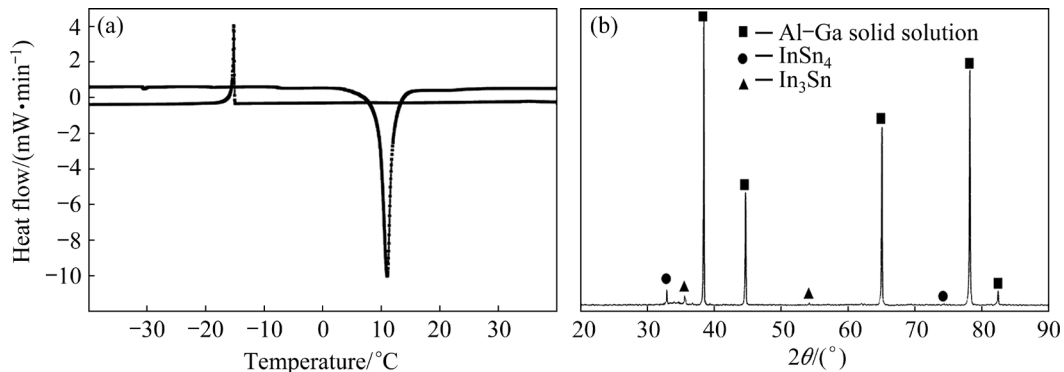


Fig. 4 DSC (a) and XRD (b) results of semi-solid Al-eGIS composites

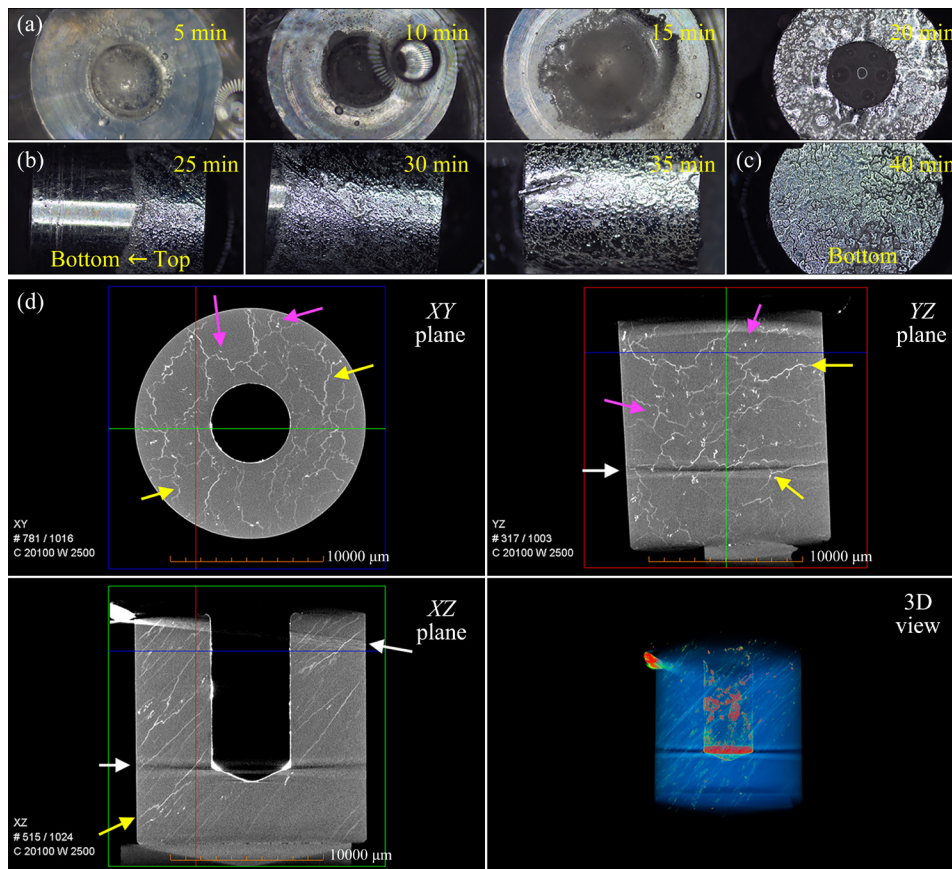


Fig. 5 Typical surface morphology evolution of Al-10wt.%eGIS composites during hydrolysis, recorded by CMOS camera at top (a), sides (b), and bottom (c); X-ray microscope reconstruction cross-sectional view (1016 projection images were collected from 0° to 360° with exposure time of 1 s and spatial resolution of $17 \mu\text{m}/\text{voxel}$) of XY, YZ, and XZ planes and 3D reconstruction image (d)

bark-type texture was subsequently observed on the top surface, providing activated sites for hydrolysis. The eGIS diffused from the top to the bottom surface (Figs. 5(b, c)) till the outer surface of Al was entirely wetted, which showed a slivery bark-type surface. The X-ray microscope images in Fig. 5(d) show that grain boundary diffusion of liquid metal occurs simultaneously where voxels belong to the diffusion path (yellow arrows), and a bark-type pattern appears, which leads to the brittle fracture of grains, while the carmine arrows corresponding to isolated white particles are metal inclusions. Due to the relatively large difference in the atomic number of Al and Ga, Ga represents higher locally enhanced absorption in a subregion of a voxel, leading to artifacts indicated by white arrows.

3.2 Typical hydrolysis process and H₂ production performance

The typical evolution of the Al–eGIS hydrolysis is represented in Fig. 6, which corresponds to the trend of curves in Fig. 7. The hydrogen bubbles immediately occurred once the campsites were exposed to water, but the initial hydrogen production was observed only from the surface of eGIS, which could be very slow due to the small amount of Al dissolved in eGIS. The production

rate increased subsequently when the eGIS started to diffuse inside and outside the Al cup. With the expansion of the activated area from the top to the bottom, the generation rate of hydrogen turned to be stable at peak value while the solution became slightly turbid colloidal. Subsequently, the LME occurred as cracks formed and bubbles tore the Al bulk into small flakes to obtain a larger specific surface area for reaction. The heat of local hydrolysis boiled water around the flakes rapidly, with H₂ bubbles carrying the water vapor out. This corrosion of Al was also accelerated by In₃Sn and InSn₄ secondary phases along the grain boundaries, which facilitated a negative shift in the Al electrode potential for the formation of micro galvanic cells [26]. Consequently, the Al cup could not be seen since most of the Al was depleted and a small amount of Al dissolved in eGIS dominated the contribution to hydrogen yield again when the Ga-rich phase formed. The solution was clearly stratified when greyish Al(OH)₃ precipitated at the bottom at the end of the reaction.

As seen from the parameters of hydrogen production performance in Table 1, Fig. 7 and Fig. 8, the yield and rate of hydrogen production increase with the rising temperature. Al–20wt.%eGIS sample reached 100% conversion in 205 min (90 °C) and 405 min (70 °C), respectively,

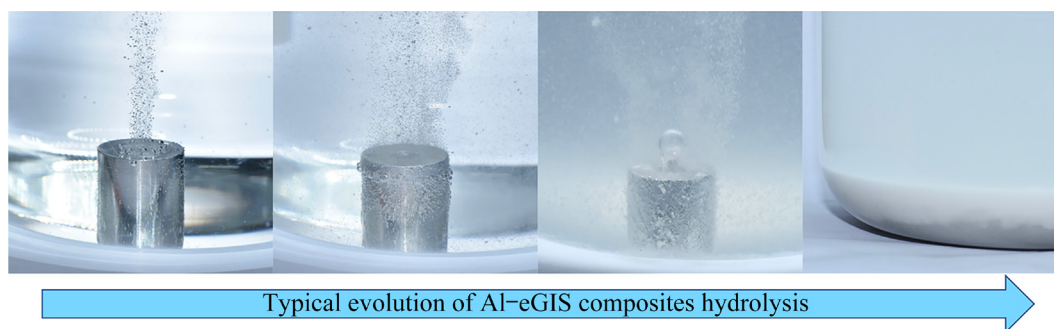


Fig. 6 Typical hydrolysis process of Al–eGIS composites

Table 1 Hydrolysis performance of Al–eGIS composites for hydrogen production

Sample No.	Composition/ wt.%	Water temperature/°C	Conversion yield/%	eGIS recovery/%	pH value of by-products
1	Al–20eGIS	50	92	48	8.5
2	Al–20eGIS	70	100	44	8.5
3	Al–20eGIS	90	100	46	8.5
4	Al–10eGIS	70	100	22	8.5
5	Al–10eGIS	90	98	21	8.5
6	Al–5eGIS	90	51	9	8.0

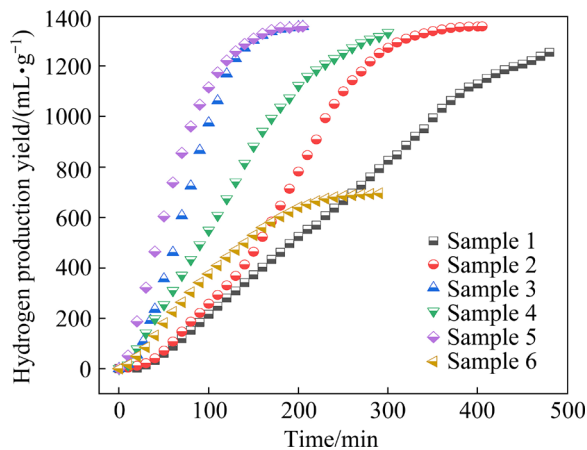


Fig. 7 Hydrogen production yield versus time of Al-*x*wt.%eGIS (*x*=5, 10, 20) composites at different temperatures

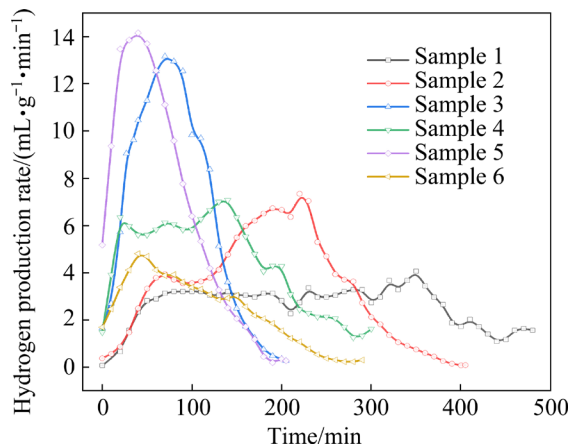


Fig. 8 Hydrogen production rate of Al-*x*wt.%eGIS (*x*=5, 10, and 20) composites at different temperatures

while it yielded at 92% in 50 °C. The Al-10wt.%eGIS sample peaked at 100% and 98% conversions at 90 and 70 °C, respectively. In contrast, Al-5wt.%eGIS (Sample 6) provided a long stable production rate as the Al cup failed to be depleted even at 90 °C, with a final conversion of 51%. For the samples that reacted thoroughly, the liquid metal recovery ranging from 21% to 44% dropped with the decreasing mass fraction of eGIS. Those recycled liquid metals can be reused in the next cycle of hydrolysis, which will greatly reduce the cost of raw materials for hydrogen production. On the other hand, despite the possible formation of alloy compounds [27,28], a small number of impurities (0.3 wt.%) in Al contributed little to the LM recovery. The pH values of all by-product solutions were in the range of 8.0–8.5, as the neutral Al(OH)₃ suspension substantially relieved

the burdens of corrosion resistance of reaction containers. On the other hand, after eGIS was isolated from the suspension, the Al can be recycled by calcinating the by-product Al(OH)₃ of hydrolysis to Al₂O₃, and then employed in the Hall–Heroult process. Moreover, the corundum (α -Al₂O₃) plays an essential role in the industry as it can be directly applied to transactions as a high-temperature resistant and wear-resisting material. Interestingly, at 90 and 70 °C, Al-10wt.%eGIS with a lower fraction of liquid metal presented faster initial and average reaction rates compared with Al-20wt.%eGIS. This was due to the relatively large reaction surface area exposed inside the blind hole when the Al cup sufficiently reacted with the eGIS, while the Al-rich phase had a shorter mass transfer path during hydrolysis.

3.3 Application in fuel cell

The generated hydrogen was connected to an experimental PEMFC for investigating the output electricity. The hydrolysis of Al-eGIS composites exhibited self-humidification, supplying humidity automatically without a humidifier. Table 2 shows relevant parameters of membrane electrode assemblies (MEA). Figure 9 displays the scheme of PEMFC. Hydrogen produced from Al-water hydrolysis catalytically split into protons and electrons on the anode (Reaction (2)), while the oxygen from the air was delivered to the cathode, forming water molecules by reacting with protons penetrated from the proton exchange membrane (Reaction (3)).



The hydrogen product from hydrolysis of Sample 5 was then applied to PEMFC. Figure 10

Table 2 Parameters of membrane electrode assemblies (MEA)

Working parameter	Value
Operating temperature/°C	70
Relative humidity/%	0
Back pressure/Pa	0
Air flow rate/(mL·min ⁻¹)	80
Working area of MEA/cm ²	3.24
N ₂ pressure/MPa	7



Fig. 9 Experimental proton exchange membrane fuel cell (PEMFC) construction: 1—Nitrogen gas pressure pump; 2—Anode heating plate (H_2); 3—Membrane electrode assemblies; 4—Cathode heating plate (Air)

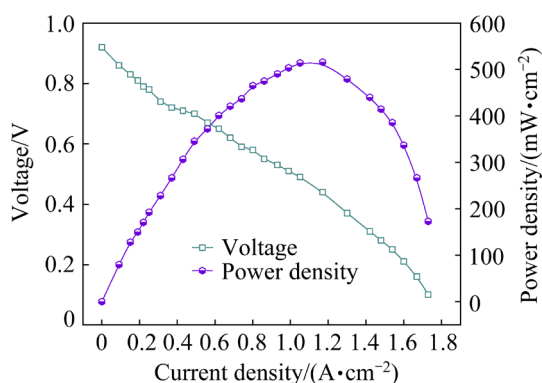


Fig. 10 Polarization curves of PEMFC

shows the polarization curves of the cell. The power density peaked at 516.05 mW/cm^2 when the current stayed at 3.8 A since the cell voltage decreased with the increment of current density. Due to the performance of the battery itself, we did not choose the current magnitude corresponding to the peak power as the constant current output in the experiment. Hence, we conducted power output measurement at the lower constant current of 1 A by considering appropriate conditions of relative humidity and mass transfer of the cell. Given a short fluctuation due to the change of H_2 concentration, the power output reached a plateau of 0.54 W for 110 min (Fig. 11), which indicated a reliable potential in the application of safe and portable electronic devices.

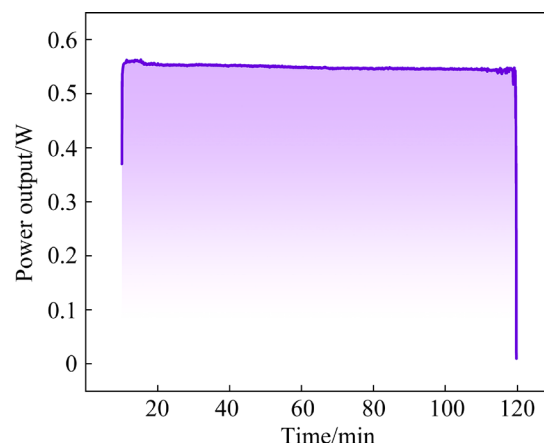


Fig. 11 Power output of PEMFC in 2 h

4 Conclusions

(1) The container design of Al-eGIS composites is conducive to easy and continuous hydrogen production via hydrolysis.

(2) The hydrolysis of Al-eGIS composites and grain boundary diffusion of liquid metal occur simultaneously with the formation of semi-solid structure, In_3Sn and $InSn_4$ secondary phases.

(3) Al-10wt.%eGIS and Al-20wt.%eGIS samples achieve nearly 100% conversion between 70 and 90°C , with a liquid metal recovery in the range from 21% to 48%.

(4) Al-10wt.%eGIS is feasible to continuously supply electricity for appliances with 0.54 W of power for 110 min by our PEMFC.

Acknowledgments

We gratefully acknowledge S. LI (Ph.D.), X. H. ZHANG and X. H. SHU for their advice and assistance throughout the course of this research. We also specially thank to M. K. WANG (Ph.D.) for the expertise on the methodology with respect to PEMFC experiments.

References

- [1] KLEBANOFF L E, KELLER J O. 5 Years of hydrogen storage research in the U.S. DOE Metal Hydride Center of Excellence (MHCoe) [J]. International Journal of Hydrogen Energy, 2013, 38: 4533–4576.
- [2] WANG Hui-hu, CHANG Ying, DONG Shi-jie, LEI Zhi-feng, ZHU Qing-biao, LUO Ping, XIE Zhi-xiong. Investigation on hydrogen production using multicomponent aluminum alloys at mild conditions and its mechanism [J]. International Journal of Hydrogen Energy, 2013, 38: 1236–1243.

- [3] GAO Zeng, JI Fei, CHENG Dong-feng, YIN Cong-xin, NIU Ji-tai, BRNIC J. Hydrolysis-based hydrogen generation investigation of aluminum system adding low-melting metals [J]. *Energies*, 2021, 14: 1433–1445.
- [4] ILYUKHINA A V, KRAVCHENKO O V, BULYCHEV B M, SHKOLNIKOV E I. Mechanochemical activation of aluminum with gallams for hydrogen evolution from water [J]. *International Journal of Hydrogen Energy*, 2010, 35: 1905–1910.
- [5] CHEN Xing-yu, ZHAO Zhong-wei, LIU Xu-heng, HAO Ming-ming, CHEN Ai-liang, TANG Zhong-yang. Hydrogen generation by the hydrolysis reaction of ball-milled aluminium–lithium alloys [J]. *Journal of Power Sources*, 2014, 254: 345–352.
- [6] FAN Mei-qiang, XU Fen, SUN Li-xian. Studies on hydrogen generation characteristics of hydrolysis of the ball milling Al-based materials in pure water [J]. *International Journal of Hydrogen Energy*, 2007, 32: 2809–2815.
- [7] NIU Feng, HUANG Xia-ni, GAO Tong, WANG Jin-gang, QIN Lai-shun, HUANG Yue-xiang. Hydrogen generation from hydrolysis of ball-milled Al/C composite materials: Effects of processing parameters [J]. *Energy Technology*, 2014, 2: 593–597.
- [8] ALINEJAD B, MAHMOODI K. A novel method for generating hydrogen by hydrolysis of highly activated aluminum nanoparticles in pure water [J]. *International Journal of Hydrogen Energy*, 2009, 34: 7934–7938.
- [9] XU Fen, SUN Li-xian, LAN Xiao-fen, CHU Hai-liang, SUN Yu-jia, ZHOU Huai-ying, LI Fen, YANG Li-ni, SI Xiao-liang, ZHANG Jian, WALTER S, GABELICA Z. Mechanism of fast hydrogen generation from pure water using Al–SnCl₂ and bi-doped Al–SnCl₂ composites [J]. *International Journal of Hydrogen Energy*, 2014, 39: 5514–5521.
- [10] LI Shu, GAN De-yu, ZHU Yun-feng, LIU Ya-na, ZHANG Ge, LI Li-quan. Influence of chloride salts on hydrogen generation via hydrolysis of MgH₂ prepared by hydriding combustion synthesis and mechanical milling [J]. *Transactions of Nonferrous Metals Society of China*, 2016, 26: 152–9. 2017, 27: 562–568.
- [11] MA Guang-lu, DAI Hong-bin, ZHUANG Da-wei, XIA Hai-jie, WANG Ping. Controlled hydrogen generation by reaction of aluminum/sodium hydroxide/sodium stannate solid mixture with water [J]. *International Journal of Hydrogen Energy*, 2012, 37: 5811–5816.
- [12] DUPIANO P, STAMATIS D, DREIZIN E L. Hydrogen production by reacting water with mechanically milled composite aluminum-metal oxide powders [J]. *International Journal of Hydrogen Energy*, 2011, 36: 4781–4791.
- [13] HUANG Hai-jun, SHU Da. Hydrogen production using AlGaInSn alloy with semi-solid structures [J]. *International Journal of Hydrogen Energy*, 2021, 46: 32595–32601.
- [14] WANG Fan-qiang, WANG Hui-hu, WANG Jian, LU Jia, LUO Ping, CHANG Ying, MA Xin-guo, DONG Shi-jie. Effects of low melting point metals (Ga, In, Sn) on hydrolysis properties of aluminum alloys [J]. *Transactions of Nonferrous Metals Society of China*, 2016, 26: 152–159.
- [15] HE Tian-tian, WANG Wei, CHEN Wei, CHEN De-min, YANG Ke. Influence of In and Sn compositions on the reactivity of Al–Ga–In–Sn alloys with water [J]. *International Journal of Hydrogen Energy*, 2017, 42: 5627–5637.
- [16] AN Qi, HU Hong-yu, LI Nan, WEI Ji-lun, WEI Cun-di, WANG Hong-chao, WOODALL J M, GAO Qian. Strategies for improving flow rate control of hydrogen generated by Al-rich alloys for on-board applications [J]. *International Journal of Hydrogen Energy*, 2019, 44: 27695–27703.
- [17] HUANG Tian-ping, GAO Qian, LIU Dan, XU Shao-nan, GUO Chun-bin, ZOU Jing-jing, WEI Cun-di. Preparation of Al–Ga–In–Sn–Bi quinary alloy and its hydrogen production via water splitting [J]. *International Journal of Hydrogen Energy*, 2015, 40: 2354–2362.
- [18] EOM K S, KIM M J, OH S K, CHO E N, KWON H S. Design of ternary Al–Sn–Fe alloy for fast on-board hydrogen production, and its application to PEM fuel cell [J]. *International Journal of Hydrogen Energy*, 2011, 36: 11825–11831.
- [19] MAHMOODI K, ALINEJAD B. Enhancement of hydrogen generation rate in reaction of aluminum with water [J]. *International Journal of Hydrogen Energy*, 2010, 35: 5227–5232.
- [20] GUAN Xu, ZHOU Zheng, LUO Ping, WU Feng-shun, DONG Shi-jie. Hydrogen generation from the reaction of Al-based composites activated by low-melting-point metals/oxides/salts with water [J]. *Energy*, 2019, 188: 116107–116117.
- [21] NASEEM K, ZHONG Hao, WANG Hui, OUYANG Liu-zhang, ZHU Min. Promoting Al hydrolysis via MgH₂ and NaOH addition [J]. *Journal of Alloys and Compounds*, 2020, 831: 154793–154800.
- [22] ZHAO Chong, XU Fen, SUN Li-xian, CHEN Jun, GUO Xiao-lei, YAN Er-hu, YU Fang, CHU Hai-liang, PENG Hong-liang, ZOU Yong-jin, LIU Zong-wen, LI Fu-wei. A novel Al–BiOCl composite for hydrogen generation from water [J]. *International Journal of Hydrogen Energy*, 2019, 44: 6655–6662.
- [23] YU Yang, WANG Shun-qi, WANG Xue-lin, WANG Qian, LIU Jing. Semisolid Al–Ga composites fabricated at room temperature for hydrogen generation [J]. *RSC Advances*, 2020, 10: 10076–10081.
- [24] XU Shuo, CUI Yun-tao, YANG Li-xiang, LIU Jing. Instant hydrogen production using Ga–In–Sn–Bi alloy-activated Al-water reaction for hydrogen fuel cells [J]. *Journal of Renewable and Sustainable Energy*, 2020, 12: 014701–014709.
- [25] ABDEL-BASET T, BENJAMIN T, BORUP R, MARTIN K E, GARLAND N, HIRANO S, KOPASZ J, LAKSHMANMN B, MASTEN D, MEHALL M. The US department of energy (DOE) [J]. *Energy Efficiency and Renewable Energy*, 2017, 1: 3–26.
- [26] DU PREEZ S P, BESSARABOV D G. Hydrogen generation by means of hydrolysis using activated Al–In–Bi–Sn composites for electrochemical energy applications [J]. *International Journal of Electrochemical Science*, 2017, 12: 8663–8682.
- [27] HE Tian-tian, CHEN Wei, WANG Wei, DU San-ming, DENG Si-er. Microstructure and hydrogen production of the rapidly solidified Al–Mg–Ga–In–Sn alloy [J]. *Journal of*

Alloys and Compounds, 2020, 827: 154290–154297.

aluminum with four liquid metals to generate hydrogen in

[28] TAN Si-cong, GUI Han, YANG Xiao-hu, YUAN Bin, ZHAN Shi-hui, LIU Jing. Comparative study on activation of

alkaline solution [J]. International Journal of Hydrogen Energy, 2016, 41: 22663–22667.

铝-共晶镓铟锡复合材料水解制氢

梁刚强^{1,2}, 刘源^{1,2}, 陈鹏飞^{1,2}, 周灿旭^{1,2}, 万坦^{1,2}

1. 清华大学 材料学院, 北京 100084;

2. 清华大学 先进成形制造教育部重点实验室, 北京 100084

摘要: 提出一种利用铝和液态金属共晶镓铟锡(eGIS)持续产生氢气的新方法。以带有盲孔的圆柱体铝作为盛放液态金属的容器, 通过水解释放氢气, 而以 eGIS 作为触发反应的窗口, 促进反应的进行。同时, 对半固态 Al-eGIS 复合材料的显微组织、水解演化和产氢性能进行研究。结果表明, 当 eGIS 沿晶界扩散到多晶铝中时, 液态金属发生脆化现象, 提高了水解过程中复合材料的反应活性, 同时观察到 In_3Sn 和 InSn_4 第二相的形成, 其有助于加快铝的水解。此外, Al-10wt.%eGIS 和 Al-20wt.%eGIS 复合材料的水解转化率接近 100%。样品应用于质子交换膜燃料进行性能测量, 在 0.54 W 输出功率下稳定供电 110 min。

关键词: 制氢; 水解; 铝基复合材料; 液态金属

(Edited by Wei-ping CHEN)